ANALYTICAL STUDY OF SORET AND DUFOUR EFFECTS ON HEAT DESTRUCTIVE CASSON LIQUID MOVEMENT PAST AN INFINITE VERTICAL PLATE

M. Venkateswarlu[1*], P. Rami Reddy[2] and K. Jaya Lakshmi[3]

[1]Department of Mathematics, V. R. Siddhartha Engineering College, Vijayawada, Andhra Pradesh, India, PIN : 520 007.
Email : mvsr2010@gmail.com
[2]Department of Mathematics, Krishna University, Machilipatnam, Andhra Pradesh, India, PIN : 522 237.
Email : ramireddyparis@gmail.com
[3]Department of Mathematics, JNTUA University, Anantapur, Andhra Pradesh, India, PIN : 515 002.
Email : jayalakshmikaramsi@gmail.com

Abstract:

This article describes a scientific solution of an unsteady movement of a Casson liquid in an infinite vertical plate in the proximity of Soret and Dufour implementations. The non-dimensional structure of mathematical equations is integrated with convenient initial and boundary limitations by applying Laplace transform technique. The expressions for Casson liquid motion, temperature, concentration, Skin-friction, heat and mass transfer coefficients are displayed. In the course of discussions, the effects of main parameters are described. The liquid motion, temperature, and concentration profiles are presented graphically for Pr = 1 and Sc = 0.22 as well as for arbitrary values of other parameters. There is no considerable difference on the effects of Soret and Dufour parameters on the liquid motion. The study is significant in the application areas of chemical analysis and biological analysis, drug delivery, bacteria detection and some others. A comparative analysis of the current research with previously published work is presented.

Keywords: Casson liquid, heat absorption, Soret effect, Dufour effect.

NOMENCLATURE

C	liquid species concentration	T	liquid temperature (K)
C_∞	uniform concentration	T_∞	uniform temperature (K)
Cf	skin friction coefficient	t	dimensional time (s)
D_m	mass diffusivity coefficient ($m^2\, s^{-1}$)	U	A scaled velocity ($m\, s^{-1}$)
D^*	dimensional Dufour number	u	fluid velocity in $x-$ direction ($m\, s^{-1}$)
D_m	non-dimensional Dufour number	u_0	characteristic velocity ($m\, s^{-1}$)
g	acceleration due to gravity ($m\, s^{-2}$)	v	fluid velocity in $y-$ direction ($m\, s^{-1}$)
H	non- dimensional heat absorption parameter		
k_T	thermal conductivity of the fluid($W\, m^{-1}\, K^{-1}$)	*Greek symbols*	
N	buoyancy ratio	β	Casson liquid parameter
Nu	heat transfer coefficient	β_T	coefficient of thermal expansion
p	Laplace Transform parameter	β_C	coefficient of concentration expansion
Pr	Prandtl number	ρ	liquid density ($kg\, m^{-3}$)
Q_0	dimensional heat generation	τ	non dimensional time (s)
q_w	heat flux	η	A scaled coordinate (m)
S^*	dimensional Soret number	θ	A scaled temperature (K)
Sc	Schmidt number	ϕ	A scaled concentration
Sr	non-dimensional Soret number	v	kinematic viscosity($m^2\, s^{-1}$)
Sh	mass transfer coefficient		

1. Introduction

In the Newtonian liquid replica several flow peculiarities are not explainable; hence the understanding of the non Newtonian liquid pattern is beneficial. Non Newtonian liquid establishes non-linear association betwixt of shear strain and rate of the shear stress. In publications, distinct patterns are accessible for non-Newtonian liquids such as Casson pattern, Jeffrey pattern, Maxwell pattern, Kelvin pattern, Burger pattern, Oldroyd-B pattern, second grade pattern, third grade pattern, and fourth grade pattern. Casson fluid pattern was developed by Casson (1959). Poornima et al. (2015) reported the radiation and chemical reaction contributes on Casson non-Newtonian liquid in the proximity of thermal and Navier slip constraints towards a stretching facade. Aboalbashari et al. (2015) obtained the entropy formation equation in terms of velocity, temperature, and concentration gradients. Makinde and Eegunjobi (2016) observed that the influence of magnetic domain and Casson liquid parameter have significant reaction on the entropy generation rate. Reddy et al. (2018) performed the hydromagnetic stream of Casson nanoliquid towards a cylinder in the proximity of first order velocity, thermal, and concentration Biot conditions. Mami and Bouaziz (2018) considered the effect of MHD on nanofluid flow, heat and mass transfer over a stretching surface embedded in a porous medium. Shashikumar et al. (2019) informed that the entropy production rate escalates with an enhancement in radiation parameter and Biot number. Gireesha et al. (2019) presented the entropy production and heat transmit inspection of Casson liquid stream in the proximity of viscous and Joule warming in an inclined micro-porous-channel. Kalyan Kumar and Srinivas (2019) presented the consequence of joule warming and radiation on unsteady MHD stream of chemically responding Casson liquid through a slantwise stretching plate. Asogwa et al. (2022) reported the suction effect on the dynamics of EMHD Casson nanofluid over an induced stagnation point flow of stretchable electromagnetic plate with radiation and chemical reaction. Reddy et al. (2022, 2023) discussed the MHD heat and mass transfer stagnation point nanofluid flow along a stretching sheet influenced by thermal radiation. Babitha et al. (2023) discussed the MHD Casson and Carreau fluid flow through a porous medium with variable thermal conductivity in the presence of suction/injection.

The Soret-Dufour factor recreates a significant role in the transmission of heat and mass on a departing liquid. It has a crucial role in various operations which involve the groundwater pollutant migration, manufacture of rubber and plastic sheets, design of nuclear reactors, geothermal energy oil reservoirs, isotopes separation, the mixture of gases, nuclear waste disposal, and compact heat insulation exchanger. Cheng (2011) represented the heat and mass transfer characteristics as functions of Lewis number, buoyancy ratio, dimensionless amplitude, thermal diffusion parameter, and diffusion thermo parameter. Ali et al. (2016) analyzed the thermal diffusion and diffusion thermo impacts on radiative MHD viscoelastic liquid motion through a porous stretching sheet. Vedavathi et al. (2017) discussed the heat transfer on MHD nanofluid flow over a semi infinite flat plate embedded in a porous medium with heat source and diffusion thermo effect. Venkateswarlu et al. (2020) presented the thermodynamic analysis of Hall current and Soret number on hydromagnetic couette flow in a rotating system with a convective boundary condition. Shaheen et al. (2021) reported the transfer of heat and mass is enhanced by inspecting the impression of the Soret and Dufour parameters with robin conditions. Ramudu et al. (2022) observed that depreciate heat transfer and appreciate mass transfer with the upsurge in Soret parameter, whereas a negative impact is perceived with Dufour parameter. Dharmaiah et al. (2022) presented the Hall and ion slip impact on magneto-titanium alloy nanoliquid with diffusion thermo and radiation absorption. Consequently, exploration in this regard with different physical aspects can be seen in refs EI-Kabeir et al. (2010); Ramzan et al. (2016); Venkateswarlu et al. (2019); Shojaei et al. (2019); Venkateswarlu and Lakshmi (2021); Jawad et al. (2021).

The objective of the present work is to record the effects of pertinent parameters administrating the Casson liquid motion and to discuss the work of Jha and Gambo (2019) as a particular case. They are not considered the impact of heat absorption. The following strategy is pursued in the rest of the article. Section two presents the mathematical model. The analytical solutions are presented in section three. Results are discussed in section four and finally section five provides a conclusion of the paper.

2. Mathematical Model

In this report, we contemplate an unsteady double diffusive natural convection movement of a Casson liquid in the proximity of heat absorption.

1. The $x-$axis is taken along the plate in the upward direction and the $y-$axis is taken normal to it.

2. At time $t = 0$, the plate and the liquid are at rest having the constant temperature T_∞ and the uniform concentration C_∞.

3. At time $t > 0$, the plate is set into motion with a velocity u_0 in upward direction. At time $t > 0$, the temperature and the concentration domains are preserved at T_0 and C_0 separately.

4. All physical quantities depend on y and t only because the plate that occupies the plane $y = 0$ is contrived to have an infinite length. The physical situation is depicted in Fig. 1.
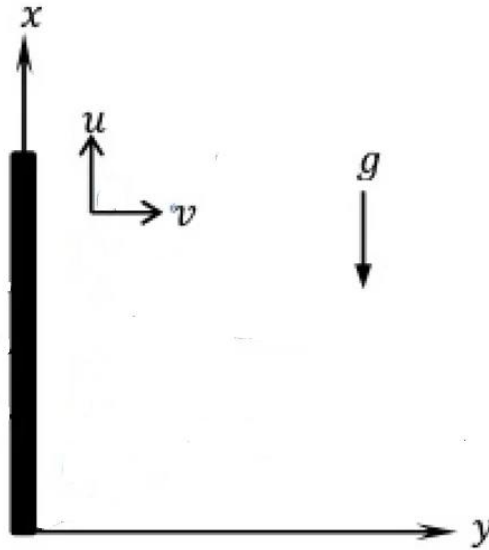

Fig. 1: Sketch of an infinite vertical plate.

The rheological equation of extra stress tensor for an isotropic and incompressible stream of a Casson liquid can be expressed as in Venkateswarlu et al. (2020, 2022).

$$\tau_{ij} = \begin{cases} 2\left(\mu_B + P_y / \sqrt{2\pi}\right)e_{ij}, & \pi > \pi_c \\ 2\left(\mu_B + P_y / \sqrt{2\pi_c}\right)e_{ij}, & \pi < \pi_c \end{cases}$$

Here μ_B is the plastic dynamic viscosity of non-Newtonian liquid, P_y is the yield stress of the liquid, π is the product of the component of the deformation rate with itself, namely, $\pi = e_{ij}e_{ij}$, e_{ij} is the (i, j) th component of the deformation rate, and π_c is the critical value of π based on non-Newtonian model.

The equations administrating the Casson liquid movement under such foundations and Boussinesq simulation in the proximity of Soret and Dufour contributes can be expressed as (see, Jha and Gambo, 2019)

Momentum conservation equation:

$$\frac{\partial u}{\partial t} = v\left(1 + \frac{1}{\beta}\right)\frac{\partial^2 u}{\partial y^2} + g\left(T - T_\infty\right)\beta_T + g\left(C - C_\infty\right)\beta_C \tag{1}$$

Energy conservation equation:

$$\frac{\partial T}{\partial t} = \frac{k_T}{\rho c_p}\frac{\partial^2 T}{\partial y^2} + D^*\frac{\partial^2 C}{\partial y^2} - \frac{Q_0\left(T - T_\infty\right)}{\rho c_p} \tag{2}$$

Mass conservation equation:

$$\frac{\partial C}{\partial t} = D_m\frac{\partial^2 C}{\partial y^2} + S^*\frac{\partial^2 T}{\partial y^2} \tag{3}$$

The initial and boundary restrictions in dimensional pattern can be written as (see, Jha and Gambo, 2019)

$$\left.\begin{array}{l} t = 0: u = 0, T = T_\infty, C = C_\infty \text{ for } y \geq 0 \\ t > 0: u = u_0, \ T = T_w, \ C = C_w \text{ at } y = 0 \\ \qquad u \to 0, T \to T_\infty, C \to C_\infty \text{ as } y \to \infty \end{array}\right\} \tag{4}$$

The successive non-dimensional variables are initiated

$$u_0 = \left[g\left(T_w - T_\infty\right)\beta_T \nu \right]^{1/3}, \theta = \frac{T - T_\infty}{T_w - T_\infty}, \phi = \frac{C - C_\infty}{C_w - C_\infty}, Y = \frac{u_0}{\nu}y, \tau = \frac{u_0^2}{\nu}t, U = \frac{u}{u_0} \tag{5}$$

Eqs. (1), (2), and (3) modified to the subsequent non-dimensional pattern

$$\frac{\partial U}{\partial \tau} = \left(1 + \frac{1}{\beta}\right)\frac{\partial^2 U}{\partial Y^2} + \theta + N\phi \tag{6}$$

$$\frac{\partial \theta}{\partial \tau} = \frac{1}{Pr}\frac{\partial^2 \theta}{\partial Y^2} + \frac{Dr}{Pr}\frac{\partial^2 \phi}{\partial Y^2} - \frac{H}{Pr}\theta \tag{7}$$

$$\frac{\partial \phi}{\partial \tau} = \frac{1}{Sc}\frac{\partial^2 \phi}{\partial Y^2} + \frac{Sr}{Sc}\frac{\partial^2 \theta}{\partial Y^2} \tag{8}$$

Here $N = \dfrac{g\left(C_w - C_\infty\right)\beta_C}{g\left(T_w - T_\infty\right)\beta_T}$, $Dr = \dfrac{D^*\left(C_w - C_\infty\right)\rho c_p}{\left(T_w - T_\infty\right)k_T}$, $Pr = \dfrac{\nu \rho c_p}{k_T}$, $H = \dfrac{Q_0 \nu^2}{k_T u_0^2}$, $Sc = \dfrac{\nu}{D_m}$, and $Sr = \dfrac{S^*\left(T_w - T_\infty\right)}{D_m\left(C_w - C_\infty\right)}$.

The consequent initial and boundary restrictions can be written as

$$\left.\begin{array}{l} \tau = 0 : U\left(Y, \tau\right) = 0, \theta\left(Y, \tau\right) = 0, \phi\left(Y, \tau\right) = 0 \text{ for } Y \geq 0 \\ \tau > 0 : U\left(Y, \tau\right) = 1, \theta\left(Y, \tau\right) = 1, \phi\left(Y, \tau\right) = 1 \quad \text{at} \quad Y = 0 \\ \quad U\left(Y, \tau\right) \to 0, \theta\left(Y, \tau\right) \to 0, \phi\left(Y, \tau\right) \to 0 \text{ as } Y \to \infty \end{array}\right\} \tag{9}$$

Utilizing the Casson liquid motion, heat transfer, and mass transfer domains, shear stress τ_w, heat flux q_w, and mass flux j_w can be displayed as

$$\tau_w = \mu\left(1 + \frac{1}{\beta}\right)\left[\frac{\partial u}{\partial y}\right]_{y=0} \tag{10}$$

$$q_w = -k_T\left[\frac{\partial T}{\partial y}\right]_{y=0} \tag{11}$$

$$j_w = -D_m\left[\frac{\partial C}{\partial y}\right]_{y=0} \tag{12}$$

In non-dimensional pattern the friction coefficient Cf, rate of heat transfer Nu, and rate of mass transfer Sh can be measured as

$$Cf = \frac{\tau_w}{\rho u_0^2} \tag{13}$$

$$Nu = \frac{\nu}{u_o}\frac{q_w}{k_T\left(T_w - T_\infty\right)} \tag{14}$$

$$Sh = \frac{\nu}{u_o}\frac{j_w}{D_m\left(C_w - C_\infty\right)} \tag{15}$$

Utilizing the Eqs. (10) to (12) into Eqs. (13) to (15), we acquired

$$Cf = \left(1 + \frac{1}{\beta}\right)\left[\frac{\partial U}{\partial Y}\right]_{Y=0} \tag{16}$$

$$Nu = -\left[\frac{\partial \theta}{\partial Y}\right]_{Y=0} \tag{17}$$

$$Sh = -\left[\frac{\partial \phi}{\partial Y}\right]_{Y=0} \tag{18}$$

3. Analytical Solution

In order to acquire analytical solutions to the coupled Eqs. (6) - (8), we adopt a small non-zero parameter ε to decouple the equations (see, Venkateswarlu et al., 2020).

$$U\left(Y, \tau\right) = U_0\left(Y, \tau\right) + \varepsilon U_1\left(Y, \tau\right) \tag{19}$$

$$\theta\left(Y, \tau\right) = \theta_0\left(Y, \tau\right) + \varepsilon \theta_1\left(Y, \tau\right) \tag{20}$$

$$\phi(Y,\tau) = \phi_0(Y,\tau) + \varepsilon\phi_1(Y,\tau) \tag{21}$$

On substituting Eqs. (19) - (21) into Eqs. (6) - (8), we acquired

$$\frac{\partial U_0}{\partial \tau} = \left(1 + \frac{1}{\beta}\right)\frac{\partial^2 U_0}{\partial Y^2} + \theta_0 + N\phi_0 \tag{22}$$

$$\frac{\partial \theta_0}{\partial \tau} = \frac{1}{Pr}\frac{\partial^2 \theta_0}{\partial Y^2} - \frac{H}{Pr}\theta_0 \tag{23}$$

$$\frac{\partial \phi_0}{\partial \tau} = \frac{1}{Sc}\frac{\partial^2 \phi_0}{\partial Y^2} \tag{24}$$

$$\frac{\partial U_1}{\partial \tau} = \left(1 + \frac{1}{\beta}\right)\frac{\partial^2 U_1}{\partial Y^2} + \theta_1 + N\phi_1 \tag{25}$$

$$\frac{\partial \theta_1}{\partial \tau} = \frac{1}{Pr}\frac{\partial^2 \theta_1}{\partial Y^2} + \frac{k}{Pr}\frac{\partial^2 \phi_0}{\partial Y^2} - \frac{H}{Pr}\theta_1 \tag{26}$$

$$\frac{\partial \phi_1}{\partial \tau} = \frac{1}{Sc}\frac{\partial^2 \phi_1}{\partial Y^2} + \frac{\lambda}{Sc}\frac{\partial^2 \theta_0}{\partial Y^2} \tag{27}$$

Here $Dr = k\varepsilon$ and $Sr = \lambda\varepsilon$ where k and λ are constantans of order one.
The corresponding boundary conditions can be written as

$$\left.\begin{array}{l} U_0(Y,0) = 0, \theta_0(Y,0) = 0, \phi_0(Y,0) = 0 \text{ for } Y \geq 0 \\ U_0(Y,\tau) = 1, \ \theta_0(Y,\tau) = 1, \ \phi_0(Y,\tau) = 1 \quad \text{at } Y = 0 \\ U_0(Y,\tau) \to 0, \theta_0(Y,\tau) \to 0, \phi_0(Y,\tau) \to 0 \text{ as } Y \to \infty \end{array}\right\} \tag{28}$$

$$\left.\begin{array}{l} U_1(Y,0) = 0, \theta_1(Y,0) = 0, \phi_1(Y,0) = 0 \text{ for } Y \geq 0 \\ U_1(Y,\tau) = 0, \ \theta_1(Y,\tau) = 0, \ \phi_1(Y,\tau) = 0 \quad \text{at } Y = 0 \\ U_1(Y,\tau) \to 0, \theta_1(Y,\tau) \to 0, \phi_1(Y,\tau) \to 0 \text{ as } Y \to \infty \end{array}\right\} \tag{29}$$

Now, we solve the Eqs. (22) - (27) subject to the initial and boundary restrictions in Eqs. (28) - (29) by applying Laplace transform technique.

Define $\eta = \dfrac{Y}{2\sqrt{\tau}}$ (30)

Then Eqs. (22) to (27) are transformed into the pattern

$$\frac{\partial U_0}{\partial \tau} - \frac{\eta}{2\tau}\frac{\partial U_0}{\partial \eta} - \left(1 + \frac{1}{\beta}\right)\frac{1}{4\tau}\frac{\partial^2 U_0}{\partial \eta^2} = \theta_0 + N\phi_0 \tag{31}$$

$$\frac{\partial \theta_0}{\partial \tau} - \frac{\eta}{2\tau}\frac{\partial \theta_0}{\partial \eta} - \frac{1}{4Pr\tau}\frac{\partial^2 \theta_0}{\partial \eta^2} + \frac{H}{Pr}\theta_0 = 0 \tag{32}$$

$$\frac{\partial \phi_0}{\partial \tau} - \frac{\eta}{2\tau}\frac{\partial \phi_0}{\partial \eta} - \frac{1}{4Sc\tau}\frac{\partial^2 \phi_0}{\partial \eta^2} = 0 \tag{33}$$

$$\frac{\partial U_1}{\partial \tau} - \frac{\eta}{2\tau}\frac{\partial U_1}{\partial \eta} - \left(1 + \frac{1}{\beta}\right)\frac{1}{4\tau}\frac{\partial^2 U_1}{\partial \eta^2} = \theta_1 + N\phi_1 \tag{34}$$

$$\frac{\partial \theta_1}{\partial \tau} - \frac{\eta}{2\tau}\frac{\partial \theta_1}{\partial \eta} - \frac{1}{4Pr\tau}\frac{\partial^2 \theta_1}{\partial \eta^2} + \frac{H}{Pr}\theta_1 = \frac{k}{4Pr\tau}\frac{\partial^2 \phi_0}{\partial \eta^2} \tag{35}$$

$$\frac{\partial \phi_1}{\partial \tau} - \frac{\eta}{2\tau}\frac{\partial \phi_1}{\partial \eta} - \frac{1}{4Sc\tau}\frac{\partial^2 \phi_1}{\partial \eta^2} = \frac{\lambda}{4Sc\tau}\frac{\partial^2 \theta_0}{\partial \eta^2} \tag{36}$$

The corresponding boundary conditions can be written as

$$\left.\begin{array}{l} U_0(\eta,0) = 0, \theta_0(\eta,0) = 0, \phi_0(\eta,0) = 0 \text{ for } \eta \geq 0 \\ U_0(\eta,\tau) = 1, \ \theta_0(\eta,\tau) = 1, \ \phi_0(\eta,\tau) = 1 \quad \text{at } \eta = 0 \\ U_0(\eta,\tau) \to 0, \theta_0(\eta,\tau) \to 0, \phi_0(\eta,\tau) \to 0 \text{ as } \eta \to \infty \end{array}\right\} \tag{37}$$

$$\left.\begin{array}{l} U_1(\eta,0)=0, \theta_1(\eta,0)=0, \phi_1(\eta,0)=0 \text{ for } \eta \geq 0 \\ U_1(\eta,\tau)=0, \ \theta_1(\eta,\tau)=0, \ \phi_1(\eta,\tau)=0 \ \text{ at } \eta = 0 \\ U_1(\eta,\tau)\to 0, \theta_1(\eta,\tau)\to 0, \phi_1(\eta,\tau)\to 0 \text{ as } \eta \to \infty \end{array}\right\} \tag{38}$$

$$Cf = \left(1+\frac{1}{\beta}\right)\frac{1}{2\sqrt{\tau}}\left[\frac{\partial U}{\partial \eta}\right]_{\eta=0} \tag{39}$$

$$Nu = -\frac{1}{2\sqrt{\tau}}\left[\frac{\partial \theta}{\partial \eta}\right]_{\eta=0} \tag{40}$$

$$Sh = -\frac{1}{2\sqrt{\tau}}\left[\frac{\partial \phi}{\partial \eta}\right]_{\eta=0} \tag{41}$$

The exact solution can be acquired by applying the Laplace transform technique stated as follows:

$$\overline{U}(\eta,p)=\int_0^\infty U(\eta,\tau)exp(-p\tau)\,d\tau \tag{42}$$

$$\overline{\theta}(\eta,p)=\int_0^\infty \theta(\eta,\tau)exp(-p\tau)\,d\tau \tag{43}$$

$$\overline{\phi}(\eta,p)=\int_0^\infty \phi(\eta,\tau)exp(-p\tau)\,d\tau \tag{44}$$

The integrations of Eqs. (31) – (36) with boundary restrictions in Eqs. (37) – (38), are given by

$$\begin{aligned} U_0(\eta,\tau)=&a_3\,\psi_1(0,1/a_1,\eta,\tau)+a_2\,exp(a_4\tau)\Big[\psi_1(a_4,1/a_1,\eta,\tau)-\psi_1(a_4+H/Pr,Pr,\eta,\tau)\Big]+ \\ &a_5\Big[\psi_2(1/a_1,\eta,\tau)-\psi_2(Sc,\eta,\tau)\Big]+a_2\,\psi_1(H/Pr,Pr,\eta,\tau) \end{aligned} \tag{45}$$

$$\theta_0(\eta,\tau)=\psi_1(H/Pr,Pr,\eta,\tau) \tag{46}$$

$$\phi_0(\eta,\tau)=\psi_1(0,Sc,\eta,\tau) \tag{47}$$

$$\begin{aligned} U_1(\eta,\tau)=&a_{13}\,exp(a_4\tau)\Big[\psi_1(a_4+H/Pr,Pr,\eta,\tau)-\psi_1(a_4,1/a_1,\eta,\tau)\Big]+ \\ &a_{14}\,exp(a_7\tau)\psi_1(a_7,1/a_1,\eta,\tau)-a_{15}\psi_1(0,1/a_1,\eta,\tau)+\lambda Na_9\Big[\psi_2(1/a_1,\eta,\tau)-\psi_2(Sc,\eta,\tau)\Big]- \\ &a_{16}\,exp(a_7\tau)\psi_1(a_7+H/Pr,Pr,\eta,\tau)+a_{17}\psi_1(0,Sc,\eta,\tau)-a_{17}\,exp(a_7\tau)\psi_1(a_7,Sc,\eta,\tau)- \\ &\lambda Na_{12}\psi_1(H/Pr,Pr,\eta,\tau) \end{aligned} \tag{48}$$

$$\theta_1(\eta,\tau)=ka_6\,exp(a_7\tau)\Big[\psi_1(a_7,Sc,\eta,\tau)-\psi_1(a_7+H/Pr,Pr,\eta,\tau)\Big] \tag{49}$$

$$\begin{aligned} \phi_1(\eta,\tau)=&\lambda a_6\,exp(a_7\tau)\Big[\psi_1(a_7,Sc,\eta,\tau)-\psi_1(a_7+H/Pr,Pr,\eta,\tau)\Big]+ \\ &\lambda\Big[\psi_1(0,Sc,\eta,\tau)-\psi_1(H/Pr,Pr,\eta,\tau)\Big] \end{aligned} \tag{50}$$

The analytical solutions for the liquid motion $U(\eta,\tau)$, liquid temperature $\theta(\eta,\tau)$, and species concentration $\phi(\eta,\tau)$ are displayed in the following pattern after simplification

$$\begin{aligned} U(\eta,\tau)=&a_{23}\psi_1(0,1/a_1,\eta,\tau)+ \\ &a_{24}\,exp(a_4\tau)\Big[\psi_1(a_4,1/a_1,\eta,\tau)-\psi_1(a_4+H/Pr,Pr,\eta,\tau)\Big]+ \\ &a_{25}\Big[\psi_2(1/a_1,\eta,\tau)-\psi_2(Sc,\eta,\tau)\Big]+a_{26}\psi_1(H/Pr,Pr,\eta,\tau)+ \\ &a_{19}\,exp(a_7\tau)\psi_1(a_7,1/a_1,\eta,\tau)-a_{21}\,exp(a_7\tau)\psi_1(a_7+H/Pr,Pr,\eta,\tau)+ \\ &a_{22}\psi_1(0,Sc,\eta,\tau)-a_{22}\,exp(a_7\tau)\psi_1(a_7,Sc,\eta,\tau) \end{aligned} \tag{51}$$

$$\theta(\eta,\tau)=\psi_1(H/Pr,Pr,\eta,\tau)+Dra_6\,exp(a_7\tau)\Big[\psi_1(a_7,Sc,\eta,\tau)-\psi_1(a_7+H/Pr,Pr,\eta,\tau)\Big] \tag{52}$$

$$\begin{aligned} \phi(\eta,\tau)=&\psi_1(0,Sc,\eta,\tau)+Sra_6\,exp(a_7\tau)\Big[\psi_1(a_7,Sc,\eta,\tau)-\psi_1(a_7+H/Pr,Pr,\eta,\tau)\Big]+ \\ &Sr\Big[\psi_1(0,Sc,\eta,\tau)-\psi_1(H/Pr,Pr,\eta,\tau)\Big] \end{aligned} \tag{53}$$

3.1 Skin friction coefficient: Using the Casson liquid motion, the plate friction coefficient can be expressed as

$$Cf = \left(1 + \frac{1}{\beta}\right)\left[\left(\frac{a_{34}}{2\tau\sqrt{\pi}} + \frac{a_{36}}{\sqrt{\pi}}\right) + \frac{1}{2\sqrt{\tau}}\begin{pmatrix} a_{35}\psi_3(a_4,0,\tau) + a_{37}\psi_3(0,H/Pr,\tau) + \\ a_{38}\psi_3(a_4,H/Pr,\tau) + a_{39}\psi_3(a_7,0,\tau) + \\ a_{40}\psi_3(a_7,H/Pr,\tau) \end{pmatrix}\right] \tag{54}$$

3.2 Heat transfer coefficient: Using the Casson liquid energy transmit, the heat transfer coefficient can be expressed as

$$Nu = -\frac{1}{2\sqrt{\tau}}\left[a_{31}\psi_3(a_7,H/Pr,\tau) - a_{32}\psi_3(a_7,0,\tau) - \sqrt{Pr}\,\psi_3(0,H/Pr,\tau)\right] \tag{55}$$

3.3 Mass transfer coefficient: Using the Casson liquid mass transmit, the mass transfer coefficient can be expressed as

$$Sh = -\frac{1}{2\sqrt{\tau}}\left[a_{29}\psi_3(0,H/Pr,\tau) + a_{30}\psi_3(a_7,H/Pr,\tau) - a_{28}\psi_3(a_7,0,\tau) - a_{27} - \sqrt{\frac{Sc}{\pi\tau}}\right] \tag{56}$$

The terms a_1, a_2, a_3, ...a_{40} and ψ_1, ψ_2 & ψ_3 are evaluated through the expressions given in Appendix.

4. Results and Discussion

In this article, the interactive implications of the various parameters such as Casson liquid parameter β, buoyancy parameter N, heat absorption parameter H, time τ, Dufour parameter Dr, and Soret parameter Sr on the liquid motion U, temperature θ, and concentration ϕ have been studied analytically and computed results of the analytical solutions are displayed graphically from Figs. 2 to 13. For the purposes of our numerical computations, we adopted the following parameter values: $\beta = 1$, $N = 0.5$, $\tau = 1$, $Pr = 1$, $Sc = 0.22$, $H = 1$, $Dr = 0.5$, and $Sr = 0.5$. To compare our results of skin friction coefficient with those of Jha and Gambo (2019) as a special case, we computed the numerical values of skin friction coefficient for our problem as well as those of Jha and Gambo (2019) which are presented in table 1. It is revealed from table 1, there is an excellent agreement between both the results.

Table 1: Comparison of the skin friction coefficient Cf as $N = 1$, $Pr = 0.71$, $Sc = 0.78$, $H = 0$, $\tau = 0.4$, and $\beta \to \infty$ with Jha and Gambo (2019).

Sr	Dr	Cf	
		Jha and Gambo (2019)	Present
0.00	0.15	2.762960	2.7629601
0.15	0.15	2.815850	2.8158500
0.30	0.15	2.869490	2.8694903
0.15	0.00	2.756830	2.7568300
0.15	0.15	2.815850	2.8158500
0.15	0.30	2.875640	2.8756402

The impact of Casson parameter on the liquid motion is presented in Fig. 2. It is identified that, the liquid motion escalates in a region close to the plate and declines in a region away from the plate with an enhancement in the Casson parameter. The ratio of the buoyancy forces due to the temperature and concentration is presented in Fig. 3. It is noticed that, the liquid motion depletes in a portion near to the plate and escalates in a portion away from the plate. Fig. 4 depicts the liquid motion for different estimations of the Dufour parameter. The Dufour parameter indicates the donation of concentration gradient to thermal energy flux in the liquid movement. In Fig. 4, observe that as the Dufour parameter escalates the liquid motion declines in a portion near to the plate and enhances in a portion away from the plate. In Fig. 5, we see that heat absorption escalates the liquid motion. Fig. 6 demonstrates the impact of Soret parameter on the liquid motion. The Soret parameter indicates the donation of temperature gradient to mass diffusion in the liquid movement. In Fig. 6, notice that as the Soret parameter escalates the liquid motion depletes in a portion near to the plate and enhances in a portion away from the plate. In Fig. 7, we notice that the liquid motion grow with the progress of time.
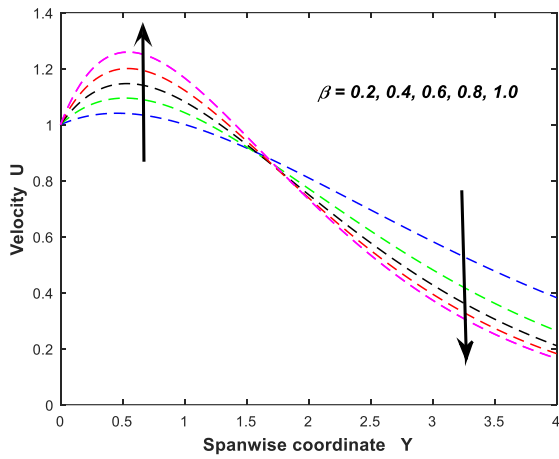
Fig. 2: Interpretation of Casson parameter on liquid motion.
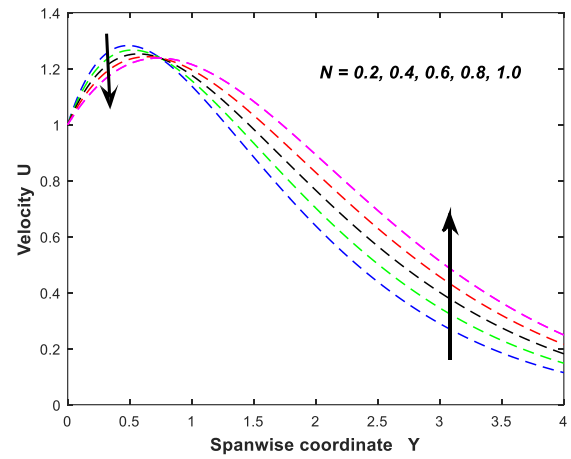

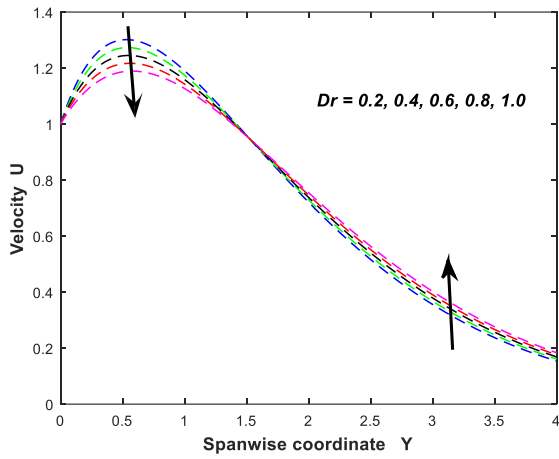Fig. 3: Interpretation of buoyancy parameter on liquid motion.

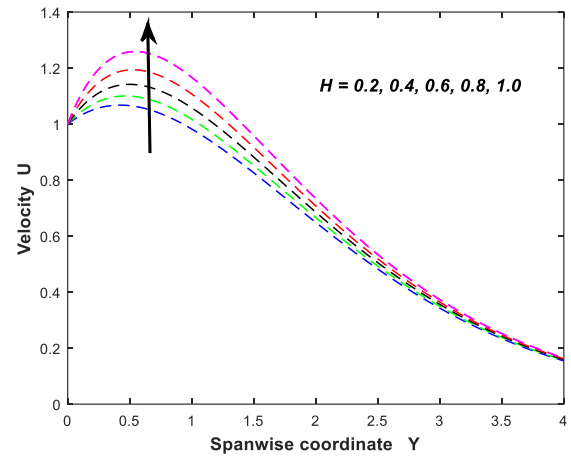Fig. 4: Interpretation of Dufour parameter on liquid motion.

Fig. 5: Interpretation of heat absorption on liquid motion.
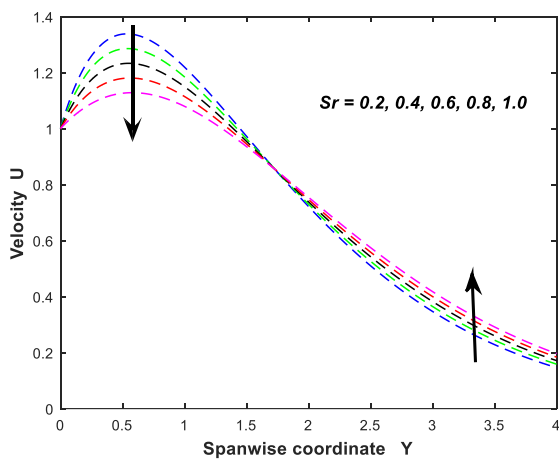

Fig. 6: Interpretation of Soret parameter on liquid motion.
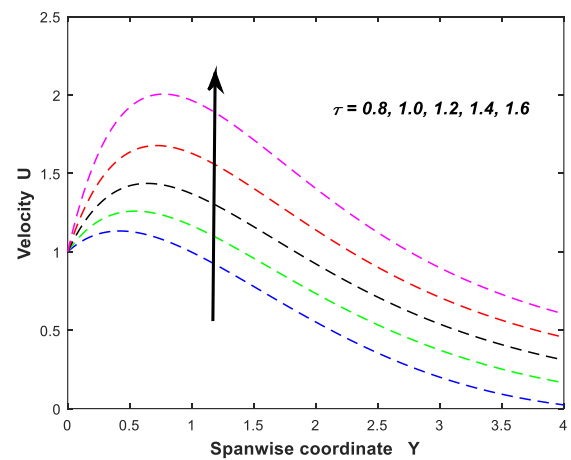

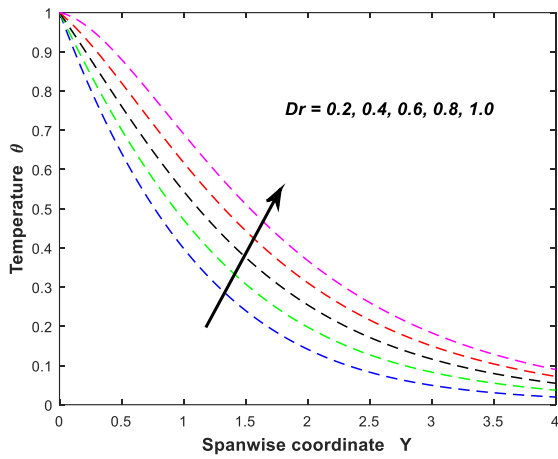Fig. 7: Interpretation of time on liquid motion.

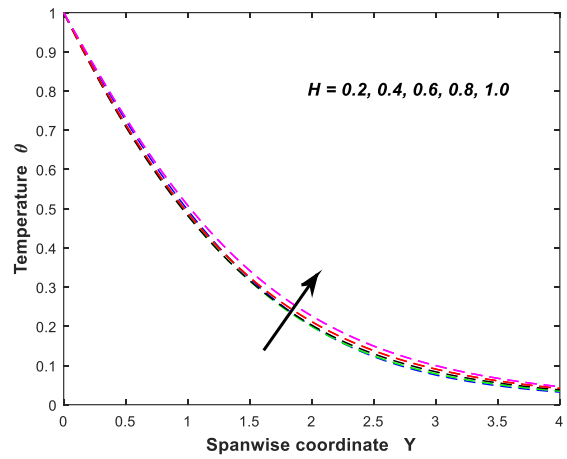Fig. 8: Interpretation of Dufour parameter on temperature.

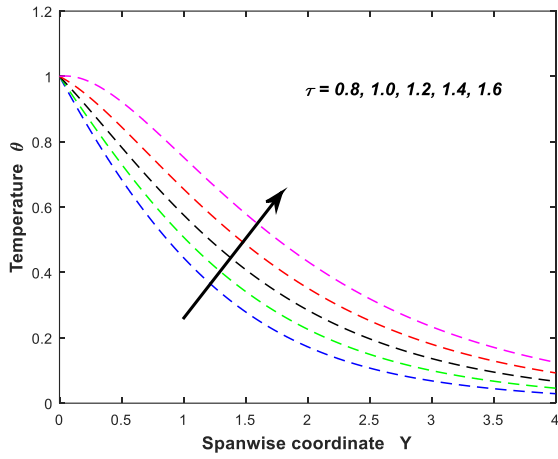Fig. 9: Interpretation of heat absorption on temperature.

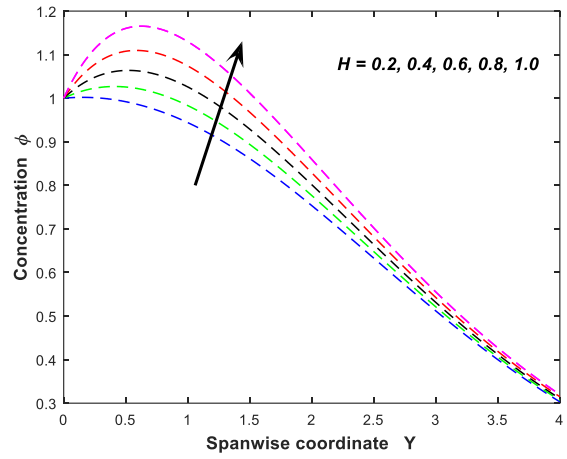Fig. 10: Interpretation of time on temperature.

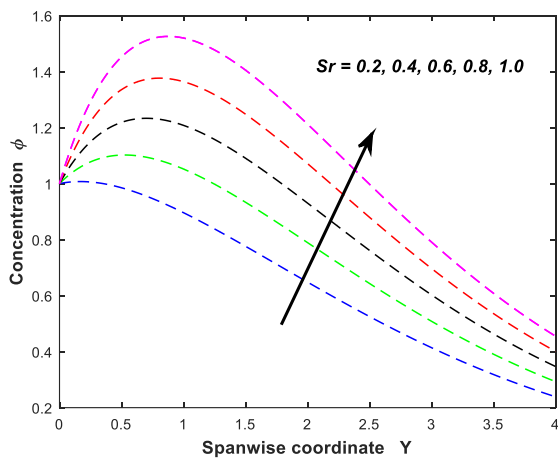Fig. 11: Interpretation of heat absorption on concentration.

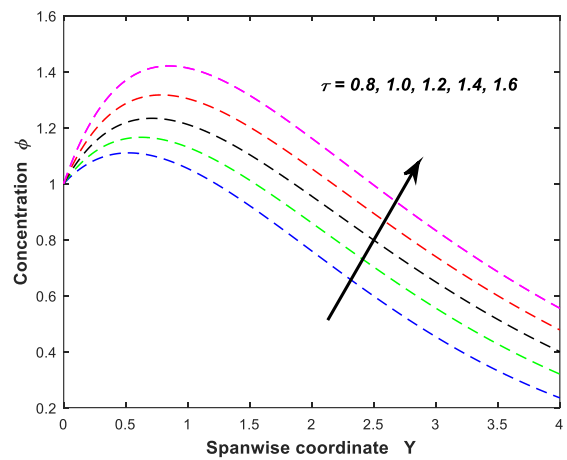Fig. 12: Interpretation of Soret parameter on concentration.

Fig. 13: Interpretation of time on concentration.

Figs. 8 and 9 depict the variation of the temperature domain with respect to Dufour and heat absorption parameters respectively. It is remarked that, the temperature domain escalates with an enhancement in the Dufour parameter or heat absorption parameter. In Fig. 10, we can observe that the temperature domain escalates with the progress of time. Figs. 11 and 12 display the impact of heat absorption and Soret parameter on the concentration domain respectively. It is noticed that, the concentration domain escalates with the accelerated values of heat absorption parameter or Soret parameter. In Fig. 13, we notice that the concentration domain escalates with the progress of time.

Table. 2: Interpretation of Cf with respect to β , N and Dr .

β	N	Dr	Cf
0.2	0.5	0.5	0.5824
0.4	0.5	0.5	0.7210
0.6	0.5	0.5	0.8418
0.8	0.5	0.5	0.9786
1.0	0.5	0.5	1.1413
1.0	0.2	0.5	1.3972
1.0	0.4	0.5	1.2266
1.0	0.6	0.5	1.0559
1.0	0.8	0.5	0.8853
1.0	1.0	0.5	0.7146
1.0	0.5	0.2	1.3770
1.0	0.5	0.4	1.2198
1.0	0.5	0.6	1.0627
1.0	0.5	0.8	0.9055
1.0	0.5	1.0	0.7483

Table. 3: Interpretation of Cf with respect to Dr , Sr and τ .

H	Sr	τ	Cf
0.2	0.5	1.0	0.3449
0.4	0.5	1.0	0.4768
0.6	0.5	1.0	0.6448
0.8	0.5	1.0	0.8609
1.0	0.5	1.0	1.1413
1.0	0.2	1.0	1.5412
1.0	0.4	1.0	1.2746
1.0	0.6	1.0	1.0080
1.0	0.8	1.0	0.7414
1.0	1.0	1.0	0.4748
1.0	0.5	0.8	0.7622
1.0	0.5	1.0	1.1413
1.0	0.5	1.2	1.5602
1.0	0.5	1.4	2.0768
1.0	0.5	1.6	2.7468

The response of Casson liquid parameter, buoyancy parameter, heat absorption parameter, Dufour parameter, Soret parameter, and time on skin friction coefficient is depicted in Tables 2 and 3. It is remarked that the skin friction coefficient depletes on escalating the buoyancy parameter, Dufour parameter, and Soret parameter however, a reverse upshot is identified on mounting Casson liquid parameter, heat absorption parameter, and time. The response of Dufour parameter, heat absorption, and time on heat transfer coefficient is portrayed in table 4. It is noticed that the heat transfer coefficient depletes on escalating the Dufour parameter and time however, a reverse upshot is identified on mounting heat absorption parameter. The behavior of Soret number, heat absorption, and time on mass transfer coefficient is displayed in Table 5. It is remarked that the mass transfer coefficient depletes on escalating the Soret parameter, heat absorption, and time.

Table. 4: Interpretation of Nu with respect to Dr, H and τ.

Dr	H	τ	Nu
0.2	1.0	1.0	0.4263
0.4	1.0	1.0	0.3274
0.6	1.0	1.0	0.2286
0.8	1.0	1.0	0.1297
1.0	1.0	1.0	0.0309
0.5	0.2	1.0	0.2785
0.5	0.4	1.0	0.2935
0.5	0.6	1.0	0.3056
0.5	0.8	1.0	0.3146
0.5	1.0	1.0	0.3200
0.5	1.0	0.8	0.3646
0.5	1.0	1.0	0.2780
0.5	1.0	1.2	0.1942
0.5	1.0	1.4	0.1038
0.5	1.0	1.6	0.0015

Table. 5: Interpretation of Sh with respect to Sr, H and τ.

Sr	H	τ	Sh
0.2	1.0	1.0	-0.0247
0.4	1.0	1.0	-0.1816
0.6	1.0	1.0	-0.3386
0.8	1.0	1.0	-0.4956
1.0	1.0	1.0	-0.6526
0.5	0.2	1.0	0.0380
0.5	0.4	1.0	-0.0178
0.5	0.6	1.0	-0.0832
0.5	0.8	1.0	-0.1622
0.5	1.0	1.0	-0.2601
0.5	1.0	0.8	-0.1989
0.5	1.0	1.0	-0.2601
0.5	1.0	1.2	-0.3180
0.5	1.0	1.4	-0.3807
0.5	1.0	1.6	-0.4554

5. Conclusions

The significant observations of this article can be listed as:
- A decreasing nature in a portion close to the plate and an increasing nature in a portion away from the plate are noticed in the liquid motion for fluctuation in the buoyancy parameter, Dufour parameter, and Soret parameter.
- The liquid motion depletes for growing values of Casson liquid parameter in a region away from the plate however, a reverse upshot is identified in a region close to the plate.
- Temperature domain augments for growing values of Dufour parameter, heat absorption, and time.
- The concentration domain escalates for larger values of heat absorption, Soret number, and time.
- Skin friction coefficient increases on escalating the Casson liquid parameter, heat absorption, and time whereas a reverse upshot is identified on mounting the buoyancy parameter, Dufour parameter, and Soret parameter.
- Heat transfer coefficient depletes on escalating the Dufour parameter and time whereas a reverse upshot is identified on mounting the heat absorption parameter.
- Mass transfer coefficient depletes on escalating the Soret parameter, heat absorption, and time.
- This study can be extending to MHD problems, porous materials, and chemical reactions.

References

Aboalbashari, M. H., Freidoonimehr, N., Nazar, F., and Rashidi, M. M. (2015): Analytical modeling of entropy generation for Casson nano-fluid flow induced by a stretching surface, Advanced Powder Technology, 26(2), pp. 542-552. https://dx.doi..org/10.1016/j.apt.2015.01.003

Ali, N., Khan, S. U., Abbas, Z., and Sajid, M. (2016): Soret and Dufour effects on hydromagnetic flow of viscoelastic fluid over porous oscillatory stretching sheet with thermal radiation, Journal of the Brazilian Society of Mechanical Sciences and Engineering, 38, pp. 2533-2546. https://dx.doi..org/10.1007/s40430-016-0506-x

Asogwa, K. K., Goud, B. S., Reddy, Y. D., and Ibe, A. A. (2022): Suction effect on the dynamics of EMHD Casson nanofluid over an induced stagnation point flow of stretchable electromagnetic plate with radiation and chemical reaction, Results in Engineering, 15, Article ID: 100518, pp. 1-9. https://dx.doi..org/10.1016/j.rineng.2022.100518

Babitha., Ramana Murthy, Ch. V., and Ramana Reddy, G. V. (2023): MHD Casson and Carreau fluid flow through a porous medium with variable thermal conductivity in the presence of suction/injection, Journal of Naval Architecture and Marine Engineering, 20(1), pp. 25–35. https://dx.doi..org/10.3329/jname.v20i1.61155

Casson, N. (1959): A flow equation for pigment-oil suspensions of the printing ink type, In Rheology of Disperse Systems, Pergamon Press, Londan, United Kingdom.

Cheng, C. Y. (2011): Soret and Dufour effects on natural convection heat and mass transfer near a vertical wavy cone in a porous medium with constant wall temperature and concentration, International Communications in Heat and Mass Transfer, 38(8), pp. 1056-1060. https://dx.doi..org/10.1016/j.icheatmasstransfer.2011.05.012

Dharmaiah, G., Sridhar, W., Balamurugan, K. S., and Kala, K. C. (2022): Hall and ion slip impact on magneto-titanium alloy nanoliquid with diffusion thermo and radiation absorption, International Journal of Ambient Energy, 43(1), pp. 3507-3517. https://dx.doi..org/10.1080/01430750.2020.1831597

El-Kabeir, S. M. M., Chamkha, A. J., and Rashad, A. M. (2010): Heat and mass transfer by MHD stagnation-point flow of a power-law fluid towards a stretching surface with radiation, chemical reaction and Soret and Dufour effects, International Journal of Chemical Reactor Engineering, 8(1). https://dx.doi..org/10.2202/1542-6580.2396

Gireesha, B. J., Srinivasa, C., Shashikumar, N., Macha, M., Singh, J., and Mahanthesh, B. (2019): Entropy generation and heat transport analysis of Casson fluid flow with viscous and Joule heating in an inclined porous microchannel, Journal of Process Mechanical Engineering, 233(5), pp. 1173-1184. https://dx.doi..org/10.1177%2F0954408919849987

Jawad, M., Saeed, A., Kumam, P., Shah, Z., and Khan, A. (2021): Analysis of boundary layer MHD darcy-forchheimer radiative nanofuid fow with Soret and Dufour effects by means of marangoni convection, Case Studies in Thermal Engineering, 23, Article ID: 100792. https://dx.doi..org/10.1016/j.csite.2020.100792

Jha, B. K., and Gambo, Y. Y. (2019): Unsteady free convection and mass transfer flow past an impulsively started vertical plate with Soret and Dufour effects: an analytical approach, SN Applied Sciences, 1, Article Number: 1234. https://dx.doi..org/10.1007/s42452-019-1246-1

Kumar, K.C. and Srinivas, S. (2019): Influence of joule heating and thermal radiation on unsteady hydromagnetic flow of chemically reacting Casson fluid over an inclined porous stretching sheet, Special Topics & Reviews in Porous Media: An International Journal, 10(4), pp. 385-400. https://dx.doi..org/10.1615/SpecialTopicsRevPorousMedia.2019026908

Makinde, O. D., and Eegunjobi, A. S. (2016): Entropy analysis of thermally radiating magnetohydrodynamic slip flow of Casson fluid in a microchannel filled with saturated porous media, Journal of Porous Media, 19(9), pp. 799-810. https://dx.doi..org/10.1615/JPorMedia.v19.i9.40

Mami, N., and Bouaziz, M. N. (2018): Effect of MHD on nanofluid flow, heat and mass transfer over a stretching surface embedded in a porous medium, Periodica Polytechnica Mechanical Engineering, 62(2), pp. 91–100. https://dx.doi..org/10.3311/PPme.10622

Poornima, T., Sreenivasulu, P., Reddy, N. B. (2015): Slip flow of Casson rheological fluid under variable thermal conductivity with radiation effects, Heat Transfer, 44(8), pp.718-737. https://dx.doi..org/10.1002/htj.21145

Ramudu, A. C. V., Kumar, K.A., Sugunamma, V., and Sandeep N. (2022): Impact of Soret and Dufour on MHD Casson fluid flow past a stretching surface with convective diffusive conditions, Journal of Thermal Analysis and Calorimetry , 147, pp. 2653-2663. https://dx.doi..org/10.1007/s10973-021-10569-w

Ramzan, M., Yousaf, F., Farooq, M., and Chung, J. D. (2016): Mixed convective viscoelastic nanofuid fow past a porous media with Soret-Dufour effects, Communications in Theoretical Physics, 66(1), pp. 133-142. https://dx.doi..org/10.1088/0253-6102/66/1/133

Reddy, M. G., Vijaya Kumari, P., and Padma, P. (2018): Effect of thermal radiation on MHD Casson nanofluid over a cylinder, Journal of Nanofluids, 7(3), pp. 428-438. https://dx.doi..org/10.1166/jon.2018.1467

Reddy, Y. D., and Mangamma, I. (2023): Influence of velocity slip and viscous dissipation on MHD heat transfer Fe_3O_4-Ethylene Glycol Nanofluid flow over a shrinking sheet with thermal radiation, Journal of Computational Biophysics and Chemistry, 22 (7), pp. 815-828. https://dx.doi..org/10.1142/S2737416523500424

Reddy, Y.D., and Goud, B. S. (2022): MHD heat and mass transfer stagnation point nanofluid flow along a stretching sheet influenced by thermal radiation, J Therm Anal Calorim, 147, pp. 11991-12003. https://dx.doi..org/10.1007/s10973-022-11430-4

Shaheen, N., Alshehri, H. M., Ramzan, M., Shah, Z., and Kumam, P. (2021): Soret and Dufour effects on a Casson nanofluid flow past a deformable cylinder with variable characteristics and Arrhenius activation energy, Scientific Reports, vol. 11, Article ID: 19282. https://dx.doi..org/10.1038/s41598-021-98898-6

Shashikumar, N. S., Prasannakumara, B. C., Archana, M., and Geerisha, B. J. (2019): Thermodynamics analysis of a Casson nanofluid flow through a porous microchannel in the presence of hydrodynamic slip: a model of solar radiation, Journal of Nanofluids, 8(1), pp. 63-72. https://dx.doi..org/10.1166/jon.2019.1568

Shojaei, A., Amiri, A. J., Ardahaie, S. S., Hosseinzadeh, K., and Ganji, D. D. (2019): Hydrothermal analysis of Non-Newtonian second grade fluid flow on radiative stretching cylinder with Soret and Dufour effects, Case Studies in Thermal Engineering, 13, Article ID: 100384. https://dx.doi..org/10.1016/j.csite.2018.100384

Vedavathi, N., Dharmaiah, G., Balamurugan, K. S., and Prakash, J. (2017): Heat transfer on MHD nanofluid flow over a semi infinite flat plate embedded in a porous medium with radiation absorption, heat source and diffusion thermo effect, Frontiers in Heat and Mass Transfer, 9(1), pp.1-8. https://dx.doi..org/10.5098/hmt.9.38

Venkateswarlu, M., and Bhaskar. P. (2020): Entropy generation and Bejan number analysis of MHD Casson fluid flow in a micro-channel with Navier slip and convective boundary conditions, International Journal of Thermofluid Science and Technology, 7(4), pp. 1-22. Paper No: 070403. https://dx.doi..org/10.36963/IJTST.2020070403

Venkateswarlu, M., and Lakshmi, D. V. (2021): Diffusion-thermo and heat source effects on the unsteady radiative MHD boundary layer slip flow past an infinite vertical porous plate, Journal of Naval Architecture and Marine Engineering, 18(1), pp. 55-72. https://dx.doi..org/10.3329/jname.v18i1.33024

Venkateswarlu, M., Bhaskar, P., and Lakshmi, D. V. (2019): Soret and Dufour effects on radiative hydromagnetic flow of a chemically reacting fluid over an exponentially accelerated inclined porous plate in presence of heat absorption and viscous dissipation, Journal of the Korean Society for Industrial and Applied Mathematics, 23(3), pp. 157-178. http://dx.doi..org/10.12941/jksiam.2019.23.157

Venkateswarlu, M., Kumar, M. P., and Makinde, O. D. (2022): Establishment of impulsive and accelerated motions of casson fluid in an inclined plate in the proximity of MHD and heat generation, Periodica Polytechnica Mechanical Engineering, 66(3), pp. 219–230. https://dx.doi..org/10.3311/PPme.19424

Venkateswarlu, M., Lakshmi, D. V., and Makinde, O. D. (2020): Thermodynamic analysis of Hall current and Soret number on hydromagnetic couette flow in a rotating system with a convective boundary condition, Heat Transfer Research, 51(1), pp. 83-101. https://dx.doi..org/10.1615/HeatTransRes.2019027139

Appendix

$a_1 = 1 + \dfrac{1}{\beta}$, $a_2 = \dfrac{1}{a_1 H}$, $a_3 = 1 - a_2$, $a_4 = \dfrac{a_1 H}{a_1 Pr - 1}$, $a_5 = \dfrac{N}{a_1 Sc - 1}$, $a_6 = \dfrac{Sc}{Pr - Sc}$, $a_7 = \dfrac{H}{Pr - Sc}$, $a_8 = \dfrac{1}{a_1 Pr - 1}$,

$a_9 = \dfrac{1}{a_1 Sc - 1}$, $a_{10} = \dfrac{a_6 a_8}{a_4 - a_7}$, $a_{11} = \dfrac{a_6 a_9}{a_7}$, $a_{12} = \dfrac{a_8}{a_4}$, $a_{13} = (k + \lambda N) a_{10} + \lambda N a_{12}$, $a_{14} = (k + \lambda N)(a_{10} + a_{11})$,

$a_{15} = (k + \lambda N) a_{11} - \lambda N a_{12}$, $a_{16} = (k + \lambda N) a_{10}$, $a_{17} = (k + \lambda N) a_{11}$, $a_{18} = (Dr + Sr N) a_{10} + Sr N a_{12}$,

$a_{19} = (Dr + Sr N)(a_{10} + a_{11})$, $a_{20} = (Dr + Sr N) a_{11} - Sr N a_{12}$, $a_{21} = (Dr + Sr N) a_{10}$, $a_{22} = (Dr + Sr N) a_{11}$,

$a_{23} = a_3 - a_{20}$, $a_{24} = a_2 - a_{18}$, $a_{24} = a_2 - a_{18}$, $a_{25} = a_5 + Sr N a_9$, $a_{26} = a_2 - Sr N a_{12}$, $a_{27} = Sr \sqrt{Sc}$, $a_{28} = a_6 a_{27}$,

$a_{29} = Sr \sqrt{Pr}$, $a_{30} = a_6 a_{29}$, $a_{31} = Dr a_6 \sqrt{Pr}$, $a_{32} = Dr a_6 \sqrt{Sc}$, $a_{33} = (Dr + Sr N) a_{10} + Sr N a_{12}$,

$a_{34} = \dfrac{a_{20} - a_3}{\sqrt{a_1}} - a_{22} \sqrt{Sc}$, $a_{35} = \dfrac{a_{18} - a_2}{\sqrt{a_1}}$, $a_{36} = \left(\sqrt{Sc} - \dfrac{1}{\sqrt{a_1}} \right)(Sr N a_9 + a_5)$, $a_{37} = (Sr N a_{12} - a_2) \sqrt{Pr}$,

$a_{38} = (a_2 - a_{33}) \sqrt{Pr}$, $a_{39} = a_{22} \sqrt{Sc} - \dfrac{a_{19}}{\sqrt{a_1}}$, $a_{40} = a_{21} \sqrt{Pr}$,

$\psi_1 (a, b, \eta, \tau) = \dfrac{1}{2} \left[exp \left(-2\eta \sqrt{ab\tau} \right) erfc(\xi_1) + exp \left(2\eta \sqrt{ab\tau} \right) erfc(\xi_2) \right]$,

$\psi_2 (a, \eta, \tau) = (2a\eta^2 + 1) \tau \, erfc \left(\eta \sqrt{a} \right) - \dfrac{2\eta \sqrt{a}}{\sqrt{\pi}} exp(-\eta^2 a)$

$\psi_3 (a, b, \tau) = \sqrt{a + b} \, exp(a\tau) erf \left(\sqrt{(a + b)\tau} \right) + \dfrac{1}{\sqrt{\pi\tau}} exp(-b\tau)$.

$\xi_1 = \eta \sqrt{b} - \sqrt{a\tau}$, $\xi_2 = \eta \sqrt{b} + \sqrt{a\tau}$